

¹ PREPARED FOR SUBMISSION TO JINST

² **Directional Xenon Measurement**

³ ABSTRACT: Abstract...

⁴ KEYWORDS: Only keywords from JINST's keywords list please

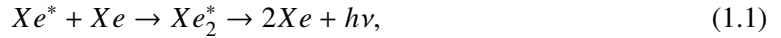
⁵ ARXIV EPRINT: [1234.56789](https://arxiv.org/abs/1234.56789)

6	Contents		
7	1	Introduction	1
8	2	Experimental Setup	2
9	2.1	The Gas Handling System	3
10	2.2	The Cryogenic System	4
11	2.3	The Detector System	6
12	2.4	The data acquisition system	7
13	2.5	The slow control system	9
14	3	Optical Properties of the Sphere	10
15	4	Detector sensitivity	11
16	5	Commissioning runs	13
17	5.1	Stability Runs	14
18	5.2	Time resolution	14
19	6	Summary	14

20 **1 Introduction**

21 The use of Noble-liquid detectors in the field of astroparticle physics has increased in the past
22 decades. Detectors aiming at measuring Dark Matter (DM) particles and neutrinos properties use
23 large liquid argon or liquid xenon (LXe) chambers [? ?]. Current and future experiment for DM
24 detection are tuned to detect weakly interacting massive particles (WIMPs), a postulated candidate
25 for DM particle [?]. LXe based detectors are to date the leading in sensitivity and size for these
26 searches [? ? ? ?].

27 When a particle interacts within the LXe media, it forms a cloud of excited and ionized states
28 with typical length of 100 nm. The excited Xe (Xe^*) combines with other Xe atoms to form excited
29 dimer states (excimers), when they decay to ground state they emit light.



30 The electrons emitted from the ionization can recombine with a surrounding atom, this process of
31 recombination provides another possibility to produce excimers,



Once Xe^* is produced it adds to the scintillation process explained in 1.1. There are two types of Xe_2^* excimer states, singlet and triplet, with lifetime of ~ 3 ns and ~ 25 ns respectively. The wavelength emitted by these states is between (175-180) nm which is lower than the lowest excitation of xenon, and therefore travel through it to reach a photo-detector situated outside the LXe. Although much is measured on these scintillation processes, the basic knowledge of the quantum properties of these interactions is based on experiments preformed several decades ago.

The phenomenon of superradiance in which identical quantum states "communicate" through an electromagnetic field if in close proximity, is well studied. In certain conditions the emission of photons from these correlated states is very different than the sum of random states. This difference is in spectral, temporal and spatial properties [? ?]. Early studies show that scintillation in LXe can produce coherent amplification of light [? ?]. These studies were focusing on the macroscopic ionization using high energy density electron beams.

The understanding and quantification of the microscopic effects of non linear phenomena such as superradiance in Lxe for a single interaction, can improve DM experiments to reduce background by the extra knowledge of directionality. Additionally irreducible background such as coherent neutrino nucleus scattering of neutrinos from the sun can be discard.

In this paper we present an experimental set-up called DIREXENO (DIREctional XENOn) aiming at measuring the spatial distribution of LXe scintillation light, and quantify non-isotropic emission.

2 Experimental Setup

In order to identify *superradiance* effects in LXe, the temporal and spatial properties of scintillation events should be studied and quantified. In the DIREXENO system LXe is circulated through a small spherical cavity held in a thick sphere made of high purity fused silica (HPFS). The sphere is surrounded ($\sim 4\pi$) by PMTs allowing high resolution, both spatial and temporal, measurements of individual photons. The PMTs do not come in contact with the xenon, so less impurities are introduced to it, and the material selection is less stringent. The geometrical design of the system approximates a point source of scintillation photons, and a detailed vertex reconstruction within the LXe bubble is unnecessary. A schematic view of the system is shown in Fig 1 .

The current system is designed with ~ 1 ns time resolution, less than 1 ns synchronization between PMTs, and ~ 0.8 radians spatial resolution. Since the exact nature and magnitude of *superradiance* in LXe is yet unknown a guiding principle in the design was flexibility to upgrades or redesign of any part of the system to fulfill any future experiment requirements. The modular design allows fast and easy recovery in case of components malfunction.

The system is made of five main building blocks. (i) **The gas handling system** which in normal working mode circulates the xenon and purifies it. (ii) **The cryogenic system**, liquefies the xenon and delivers it to the detector system. (iii) **The detector system** consists of an HPFS sphere that holds a small bubble of LXe target, and PMTs around it. (iv) **The DAQ system** supplies High Voltage (HV) to the PMTs and handles triggering and digitization of data. (v) **The slow control (SC) system** monitors the condition of the experiment using various gauges and also sends alarms if some measurements exceed normal values. The entire assembly is held on 3 separate racks as shown in Fig. 2.

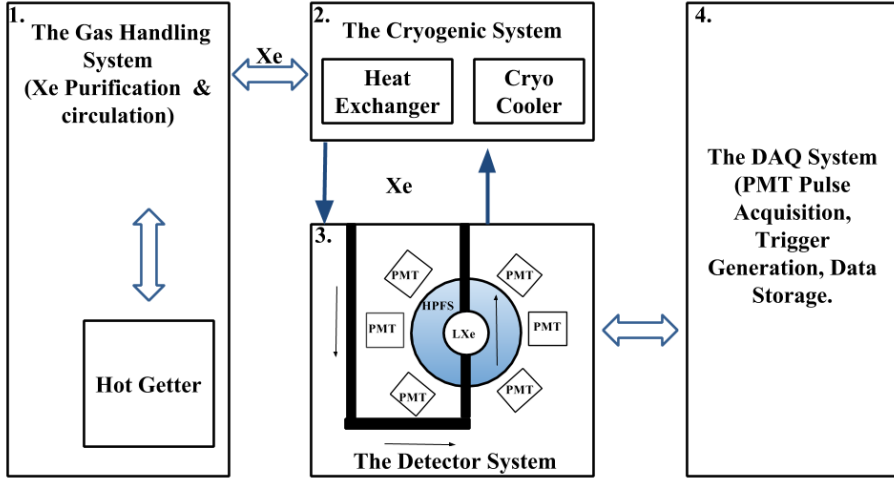


Figure 1. A schematic view of DIREXENO .

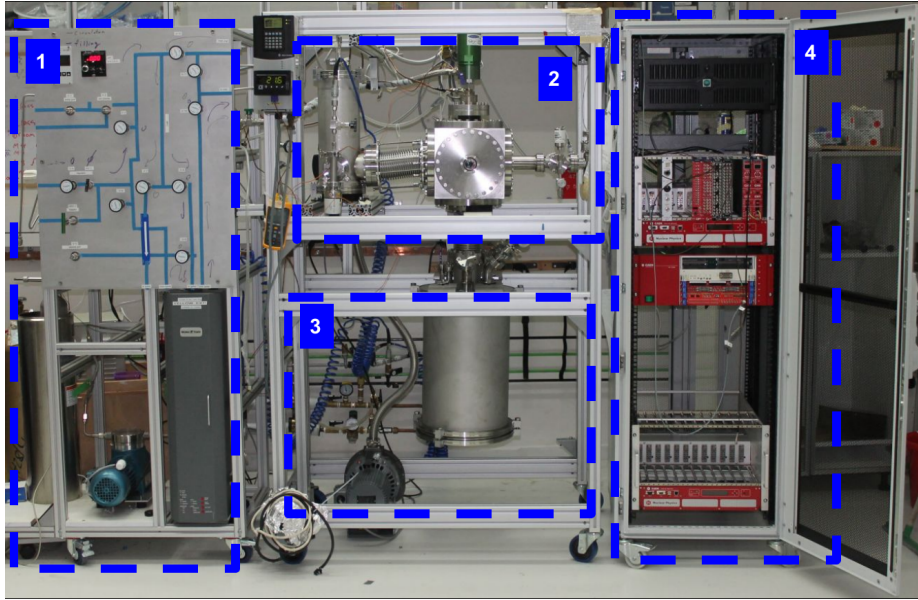


Figure 2. The DIREXENO system mounted on the three racks. 1. The gas handling system. 2. The cryogenic system including the heat exchanger. 3. The detector chamber. 4. The Data acquisition system. The SC system is distributed around all 3 racks.

73 2.1 The Gas Handling System

74 In DIREXENO , only the prompt scintillation is measured, so a high level of LXe purity is not of a
 75 great importance. However in many LXe detectors the desired level of impurity concentration is at

the level of 1 ppb O₂ equivalent [?], this is crucial to allow ionization electrons drift for several cm. To reach that purity level in a reasonable amount of time (several days instead of months), a continuous purification is needed. The gas handling system provides this process along with all gas handling operations such as filling, recuperation and circulation. The xenon circulation also plays a major role in heat transfer.

During purification, The xenon is forced by a circulation pump¹ extracting LXe from the detector part through a heat exchanger², where it is heated and vaporized, into a hot getter³ which cleans the xenon. The xenon passes through a mass flow controller⁴ (MFC), enabling monitoring and controlling the amount of heat introduced to the system. Once purified, the xenon is delivered back to the cryogenic system via the heat exchanger, where the remaining GXe is liquefied before flowing back to the detector part. A schematic of this system is shown in fig. 3.

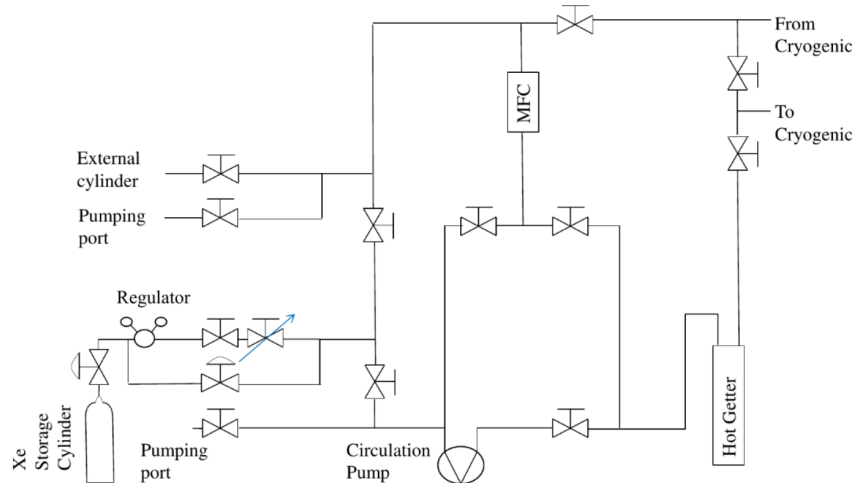


Figure 3. Schematics of the gas handling system. High pressure valves are indicated as valves with arcs. Needle valves are indicated as a valve with an arrow.

2.2 The Cryogenic System

Remote cooling is generally used in LXe experiments due to reduction in background radiation and acoustic noise from the cooler to the detector, and due to design flexibility. The cryogenic system is connected to the gas handling system on one side and to the detector part on the other, and built such that replacing the cryo-cooler type (e.g., to PTR) requires just an adaptation to the top flange.

The cryogenic system is divided to an Outer Vessel (OV) which holds the insulation vacuum, and an Inner Vessel (IV) which holds the xenon. In addition to the vacuum which prevents heat leakage due to diffusion and convection, the IV is fully covered by multi layer Aluminized Mylar to prevent heating via radiation.

The OV is made of a 10" Conflat (CF) cube, with ports on all six faces, interfacing the gas handling system and the detector part, and bearing service ports (e.g., feed-throughs, pumping

¹N143 SN.12E AC 230V50HZ KNF diaphragm circulation pump

²GEA GBS100M-24 plate heat exchanger

³MONO-TORR PS4-MT15-R-2

⁴MKS mass flow controller 1179A00614CR1BM

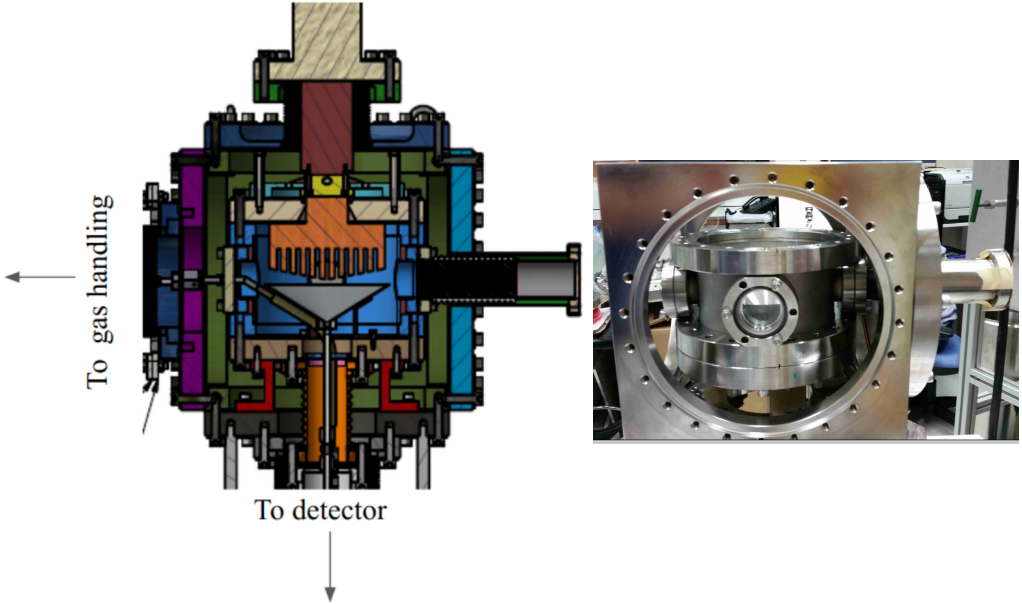


Figure 4. CAD view of the cryogenic system(Left) and a picture of the cryogenic system (Right).

98 ports, view ports). The OV is connected to the detector part via a 6" CF flexible bellows, providing
 99 a shared vacuum space.

100 The IV is made of 1.5" long cylinder with 6" CF flanges on both sides, holding xenon within.
 101 A 120 mm diameter cold finger is welded to its top flange. The design of the cold finger is similar
 102 to the one in [?]. The inner part of the cold finger is made of long fins, resulting in a better heat
 103 transport. The upper part of the cold finger is in thermal contact with the QDrive cryo-cooler ¹ via
 104 a copper adapter. A cartridge-heater is also inserted to the copper adapter for emergency heating in
 105 case xenon freezes on the cold finger.

106 The cryo-cooler is connected via a 4¹/₂" flange to the OV top flange. While usually cryo-coolers
 107 used for xenon experiments constantly operate in maximal cooling, the QDrive cryo-cooler utilizes
 108 a temperature control to vary its cooling power up to ~70 W. This allows setting a desired working
 109 temperature which is constant within less than 0.1 °C measured on the cryo-cooler.

110 On the inner side of the IV bottom flange a thin 0.6 mm Stainless Steel (SS) funnel is installed
 111 collecting LXe drops from the cold finger, and delivering them to the detector. This flange is
 112 attached to the detector part, via a 3³/₈" flexible bellows. The bellows hosts two pipes connected
 113 to the circulation system, and a third pipe coming from the funnel. The three pipes deliver LXe
 114 whereas the GXe is filling the bellows volume. The purer LXe (from the gas handling system) and
 115 the less pure LXe (from the cold finger) are separated, and can be delivered to different parts of the
 116 system. Some of the guidelines for the design of the cryogenic system are based on [?]. The CAD
 117 view of the design of the cryogenic system and a photo of the actual system are shown in Fig 4.

¹QDrive 20BB 9p6 A 3 AYNBNCO

¹¹⁸ **2.3 The Detector System**

¹¹⁹ The detector system refers to a vacuum chamber and its inner assembly consisting of a transparent
¹²⁰ sphere that contains the LXe, the PMT sensors observing it and their accessories. This chamber is
¹²¹ placed below the cryogenic system.

¹²² The interface unit to the cryogenic system is built out of two flanges welded together via seven
¹²³ tubes, which serve as service ports for electrical and other feedthroughs: four with a $2\frac{3}{4}$ " CF flange,
¹²⁴ and three with a $1\frac{1}{3}$ " CF flange (mini-CF). The upper flange, ISO-K NW320, shares the cryogenic
¹²⁵ system's OV insulation vacuum, while the bottom one, CF-10", is part of the IV and could hold
¹²⁶ xenon for future detectors. The CF flange is also adapted to fit a smaller CF- $4\frac{5}{8}$ " flange which is
¹²⁷ currently used.

¹²⁸ The vacuum chamber is made of an ISO-K NW320 nipple closed with a blank flange from
¹²⁹ below, the length of the nipple is determined such that the maximal height of the whole apparatus
¹³⁰ is 190 cm, allowing an easy transport of the detector through standard doors.

¹³¹ The $4\frac{5}{8}$ " CF flange is connected to a split vessel that serves as a LXe reservoir. One part is
¹³² connected to the top of the HPFS sphere, and one to the bottom. LXe is circulated such that LXe
¹³³ coming from the gas system drips into one part and pumped from the other. This controls the liquid
¹³⁴ level to be above the sphere, so the sphere is constantly filled with LXe.

¹³⁵ Below the sphere, another LXe reservoir serving as a thermal bath is connected holding Peter,
¹³⁶ how much is the volume of the lower pools, also I would add an Image/CAD view of the two pools.
¹³⁷ This reservoir is designed with a small XXX deg inclination so GXe bubbles which forms inside it
¹³⁸ will move towards the other direction of the sphere. In addition the pipe connected to the sphere has
¹³⁹ the shape of a snorkel so no bubbles will go inside the sphere, maintaining the sphere with liquid
¹⁴⁰ and no boiling bubbles.

¹⁴¹ The sphere is a custom designed hollow shell made of Corning HPFS 8655 with high trans-
¹⁴²mittance to VUV. Two Invar tubes with SS mini-CF flange are connected to the sphere on both
¹⁴³sides. The technical design and photo of the sphere are shown in Fig. 5. The optical properties
¹⁴⁴of the sphere will be further discussed in Sec. 3. The bottom flange of the sphere is held using a
¹⁴⁵brass holder to prevent force or torque applied on the sphere while mounting it. The brass holder is
¹⁴⁶connected to a plate held from the top CF-10" flange.

¹⁴⁷ Photons emitted from the LXe in the sphere are detected by 20 PMTs¹. The PMTs are chosen
¹⁴⁸to have a quantum efficiency greater than 30% at 178 nm. The voltage applied on each PMT (the
¹⁴⁹maximum is +900V) is adjusted such that the gain of the PMT is 2×10^6 . A positive voltage
¹⁵⁰divider² is used to provide high voltage to the PMTs. The PMTs are held with a special aluminum
¹⁵¹holder, coated with anti-reflection color. The holder is made of two hemispheres hosting the PMTs
¹⁵²in 3 rows, all of them pointing to the center of the sphere. The PMTs are attached to the holder by
¹⁵³their voltage-divider bases using M2 PEEK screws (see Fig 6). The CAD design and a photo of
¹⁵⁴the detector system are shown in Fig. 7.

¹R8520-406 Hamamatsu 1" PMT, active area 20.5 mm \times 20.5 mm

²Hamamatsu VDS18130p 24 channel positive polarity.

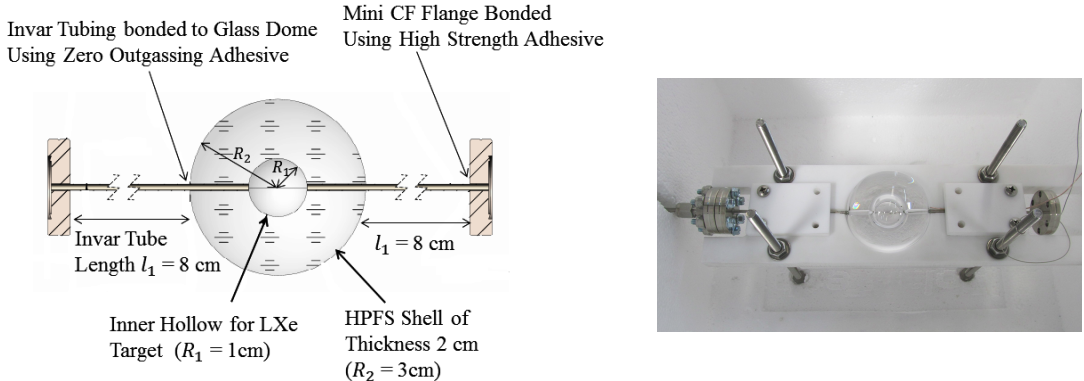


Figure 5. (Left)The technical design of the HPFS shell with Invar tubing and mini CF flanges. (Right) The industrially manufactured HPFS shell, held in a test fixture.

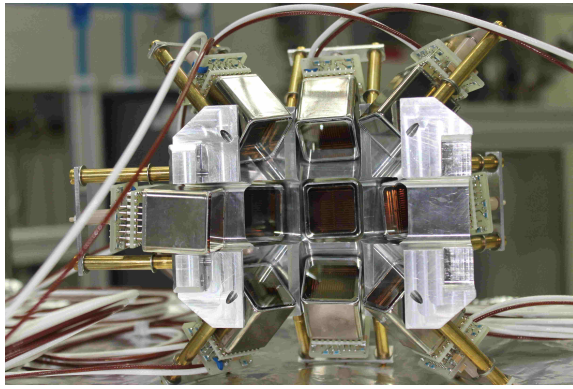


Figure 6. A PMT holder–hemisphere. Two identical hemispheres are used to hold the PMTs around the sphere.

155 2.4 The data acquisition system

156 The DAQ system is heterogeneous using both NIM and VME electronic modules. The data readout
 157 is being carried out through a PCIe card¹ connected via an optical link to a VME controller². A
 158 schematic layout of the DAQ system is shown in Fig. 8.

159 The PMTs are ramped up to their individual working voltage (corresponding to a gain of
 160 2×10^6) using VME high voltage distributor module³. The raw pulses from the PMTs are amplified
 161 and shaped using two PMT preamplifiers⁴. The preamplifier operates from DC to 275 MHz and
 162 produces two identical $50\ \Omega$ non inverting outputs with voltage gains of 10 for each PMT channel.
 163 One of the outputs is converted into a digital signal by an ADC⁵, and the other to binary signals
 164 using two discriminators⁶.

¹CAEN A3818 PCIe

²CAEN V2718 VME controller

³iseg VDS18130p : 24 independent channels positive polarity voltage distributor

⁴Phillips 776. 16 independent and direct-coupled amplifiers channels

⁵CAEN ADC V1742: switched capacitor digitizer

⁶CAEN V895 16 channel leading edge discriminator

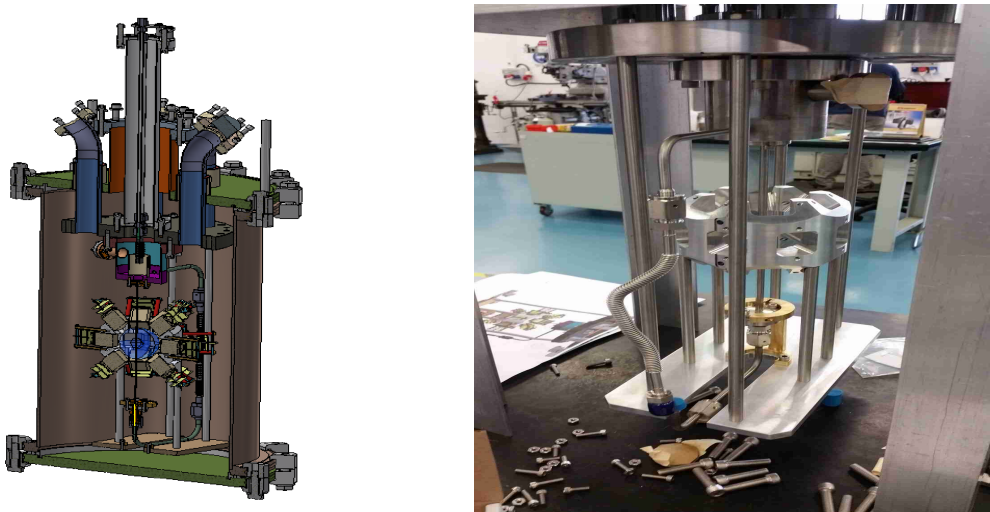


Figure 7. (Left) CAD design of the detector part. (Right) First mounting of the detector part, still not connected to the rest of the system.

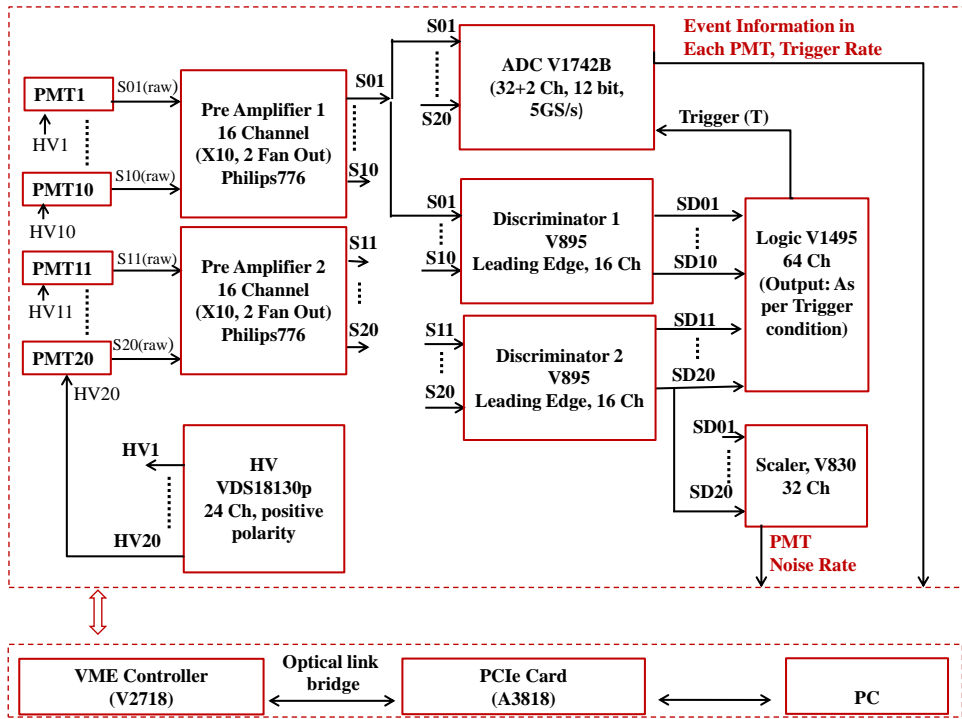


Figure 8. The schematic of the data acquisition system of DIREXENO . The signal coming from 20 PMTs ($i = 1 - 20$) and the subsequent electronic channels to record the events once triggered. Where $S_i(\text{raw})$ is the raw electrical pulse output of the PMTs, S_i are the amplified pulses, and SD_i are the binary outputs from the discriminator.

165 The ADC consists of two 12 bit 5 GS/s switched capacitor digitizer sections, each of them
 166 with 16+1 channels, based on DRS4 chip. The dynamic range of the input signal is 1 Vpp with an
 167 adjustable DC offset. This module constantly samples (5 GS/s, 2.5 GS/s or 2 GS/s) either bipolar

168 or unipolar analog input signals, and records them into circular analog memory buffers. Once
169 triggered, all analog memory buffers are frozen and digitized into a digital memory buffer with a
170 12 bit resolution. The measured rise time of the system (PMTs, bases, DAQ) is measured to be
171 (1.4 ± 0.6) ns, the measured jitter is, (390 ± 67) ps.

172 The binary output signals from the discriminator are duplicated and fed to the logic module¹
173 and to a scaler². A global majority trigger is generated in the logic module with the coincidence of
174 any two out of the twenty PMTs within a predefined time window, that will be optimized to reduce
175 dark counts. The event information and trigger rate are read from the ADC, while the individual
176 PMTs trigger rate from the scaler. Further analyses of the relevant events are carried out offline.

177 2.5 The slow control system

178 A variety of sensors collect information from the various subsystems, that is being used for monitoring
179 the stability and well-being of the system as well as understanding the complex Xe flow through
180 the system. We use a time-series server built specifically for handling events or measurements that
181 are time-stamped based on influxdb [1]. For monitoring and visualization we use Grafana [2], an
182 open source software for time series analytics. The monitored data is streamed to the database using
183 the influxdb API integrated in python control scripts.

184 Ten 100Ω pt resistors³ are installed. Two in the copper adapter attached to the cold finger,
185 and eight around the sphere, pools and pipes. The resistors are connected to a PID reader⁴ for
186 temperature measurements. To support a readout of more temperature sensors with the same
187 number of feedthroughs data channels we replaced some of the 4-wires PT100 readout channels
188 with a 2-wires one. The temperature-resistance calibration curves were shifted accordingly. The
189 lesser measurement accuracy and stability were more than sufficient to identify liquid-gas transitions
190 and temperature transients. Pressure/Vacuum reading of the outer- and inner-chamber were done
191 using xxxx and xxxx sensors. Termistors based sensors were installed on the cooling water lines,
192 the compressor and near the system for monitoring of the cryocooler operation. They were read
193 using an arduino board with an accuracy of <1 degree. The xenon flow rate readings from the MFC
194 are monitored, and a ‘homemade’ switch read by the arduino lets the operator to move between
195 Filling/Recooperation/Circulation modes to allow the proper handling of the flow rate data in the
196 data base (either adding it to the total Xe amount, removing it or no change). The PMTs voltage,
197 current and trigger rate are also monitored and streamed to the database.

198 An off-the-shelf USB snake-camera is mounted in the outer vacuum chamber and watching the
199 sphere. The camera is housed in a xx “ nipple with an optical window on one side and a xx bellow
200 on the other opened to the air side. The camera allows the operator to visually inspect the status
201 of the Xe within the sphere. A simple and fast image processing is constantly performed and the
202 difference between two consecutive optical snapshots is calculated and streamed into the data base.

203 An additional script is monitoring the database, identifies missing information or other problems
204 based on a set of rules, and alerts the operators via email and sms.

¹CAEN V1495: FPGA based general purpose VME board

²CAEN V830: 16 channel scalar

³PT111 Lakeshore

⁴cryo-con model 18i Cryogenic Temp Monitor

205 3 Optical Properties of the Sphere

206 The central component of the experiment is the HPFS sphere, which holds the LXe target, located
 207 in the center of the detector system. In order to allow the measurement of the original direction of
 208 photons emitted by the LXe, it is important to reduce the amount of diffractions and absorptions of
 209 photons on their path from the LXe to the PMTs.

210 To insure the photons emitted by the LXe can be measured by the PMTs, the HPFS transparency
 211 to VUV photons is crucial parameter for setting the sphere's dimensions (inner and outer radii).
 212 Therefore, the transmittance of an HPFS sample was measured, using the above mention VUV
 213 monochromator. The deuterium light source¹ spectrum is in the range of (110-190) nm, peaked
 214 at 160 nm was facing a vacuum space. Using a PMT placed in the vacuum, the intensity of the
 215 light is measured, both with and without the HPFS sample. The ratio of the measured intensities
 216 is converted to the transmittance of the HPFS. The transmittances as a function of wavelength are
 217 shown in Fig. 9 (right panel). The transmittance of the sample at 178 nm, is ~ 98.7 %/cm.

218 In order to reduce the diffraction in the LXe-HPFS transition, the sphere material is chosen
 219 to be HPFS, as the refractive index of its HPFS is 1.58 at 185 nm, matching to the LXe one, which
 220 is 1.61. The refractive index of this HPFS is 1.58 at 185 nm, matching to the LXe one, which is
 221 1.61. The refractive index at various wavelengths was measured in Prof. Amos Breskin's lab using
 222 a VUV monochromator². The results of these measurements are shown in Fig. 9 (left panel). The
 223 sphere is made of two HPFS hemispheres bonded together.

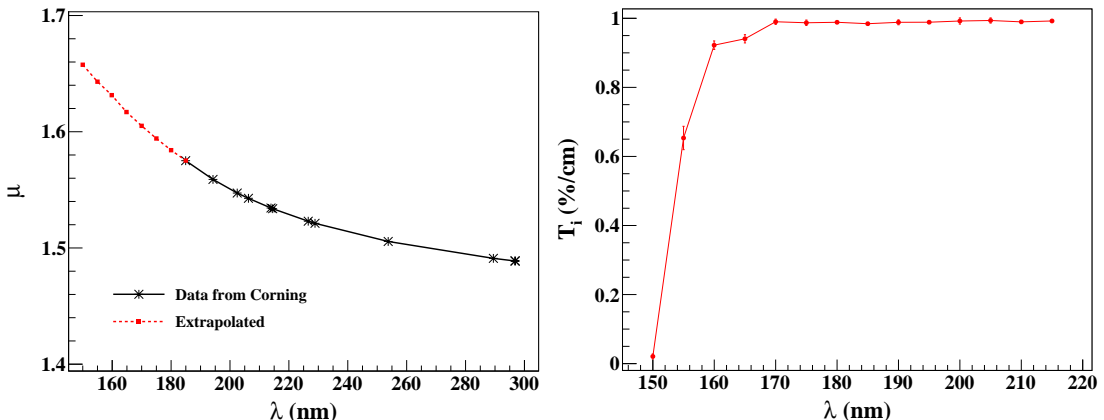


Figure 9. Some relevant characteristics of HPFS-8655. (Left) The refractive index as provided by Corning and extrapolated to relevant wavelength range. (Right) The measured internal transmittance (T_i), the mean and RMS obtained from 10 sets of measurements are shown.

224 Finally, in order to reduce the diffraction in the HPFS-Vacuum transition as well as internal
 225 reflections, the sphere should be thick so all photons will arrive in a perpendicular angle to the
 226 HPFS surface. In addition the sphere must not be too thick not to attenuate the scintillation light.
 227 The LXe target bubble within should be large to increase the detector medium but not be too large
 228 in order to avoid double scatters. Using a GEANT4 based simulation [?] studying the path of the

¹McPherson 632

²McPherson 234/302VM

229 scintillation photons the sphere dimensions are optimized. The outer radius is chosen to be 3 cm,
 230 and the inner (the hollow space that holds the LXe) is chosen to be 1 cm.

231 The sources that will be used for exciting the xenon and creating the superradiance (signal) as
 232 well as the standard emission (background), will be ^{137}Cs ($E_\gamma=662$ keV) and ^{57}Co ($E_\gamma=122$ keV &
 233 136 keV) for ER with mean free path of ~ 4 cm and ~ 1 cm respectively. For NR, $^{241}\text{AmBe}$, D-D
 234 neutron generator, or neutron produced in an accelerator will be used.

235 4 Detector sensitivity

236 The sensitivity of the detector is estimated by its ability to identify an anisotropic component in the
 237 scintillation photons emission pattern (signal), over the isotropic one (background). The photon
 238 emission pattern is modeled using a combination of isotropic emission and one or two beams

$$\mathcal{F}(\theta, \phi) = (1 - r_{aniso}) \cdot f_{iso} + r_{aniso} \cdot [r_1 f_G(\sigma_1) + r_2 f_G(\sigma_2)], \quad (4.1)$$

239 where f_{iso} is the PDF of an isotropic emission, f_G is a PDF of a Gaussian distribution with half
 240 width σ . r_{aniso} is the anisotropic emission fraction, and $r_{1,2}$ are the relative beams intensities. The
 241 first beam direction is random, and the second's is either random (“uncorrelated”) or opposite to
 242 the first's (“correlated”). The different emission patterns used here are summarized in Table 1.

Pattern no.	No. of beams	type	Beam half widths		Signal fractions		N'
			σ_1	σ_2	r_1	r_2	
1	1	single beam	5^0	-	1	0	3200
2	1	single beam	15^0	-	1	0	4630
3	2	correlated	5^0	5^0	0.5	0.5	4520
4	2	correlated	15^0	15^0	0.5	0.5	9770
5	2	uncorrelated	5^0	5^0	0.5	0.5	9370
6	2	uncorrelated	5^0	10^0	0.5	0.5	19500
7	2	uncorrelated	15^0	15^0	0.5	0.5	28200
8	2	uncorrelated	10^0	30^0	0.5	0.5	49900
9	2	uncorrelated	10^0	30^0	0.2	0.8	56000
10	2	uncorrelated	30^0	10^0	0.2	0.8	43000

Table 1. Anisotropic emission patterns. For all patterns $r_{aniso} = 0.1$

243 A GEANT4 based simulation is used to model the detector system, generate photons, propagate
 244 them through the detector, and obtain a PMT hit pattern. The photons detected at the PMTs are
 245 mapped and put through a statistical test to check the detector's sensitivity towards the different
 246 emission patterns [?].

247 The relevant geometrical and optical parameters, which are used in the simulation, are listed
 248 in Table 2. The scintillation light produced in a particular event is emitted by a cloud of excimers.
 249 This cloud is assumed to have a linear size much smaller than that of the optical system. Therefore
 250 each event is simulated as a number of photons that are emitted from a point in the LXe with
 251 some emission pattern (see Table 1). The number of generated photons for each event is taken to
 252 be Poisson(50), which correspond to an energy deposition of ~ 2.5 keV or ~ 7 keV for ER or NR

253 respectively. The LXe target is much smaller than the mean free path of the source particles, and to
 254 account for that the events are uniformly generated in the LXe volume. The probability for a photon
 255 being transmitted/reflected at a given surface is determined by Fresnel's equations, which include
 256 Snell's law for the transmitted light, and specular reflection for the reflected light. The boundary
 257 surfaces between different media such as, the LXe–HPFS, HPFS–vacuum and vacuum–PMT, are
 258 assumed to be perfectly smooth, therefore enabling only specular reflection. The photons reaching
 259 the PMTs can either be detected, absorbed or reflected from the photocathode or PMT window. A
 260 simplified approach of the above possibilities is considered: a photon reaching the PMT has a 30%
 261 probability to be detected (since the PMTs have $\text{QE} \geq 30\%$), 50% probability to get absorbed and
 262 20% probability to get specularly reflected.

Parameter	Value	Parameter	Value
LXe absorption length	100 cm	HPFS shell inner radius	1cm
LXe scattering length	35 cm	HPFS shell thickness	2 cm
LXe refractive index	1.61	PMT QE	30%
LXe Scintillation wavelength	178	PMT distance from center	39 mm
HPFS absorption length	100 cm	Number of PMT	20
HPFS refractive index	1.57	PMT active area	22mm × 22mm
HPFS scattering length	∞	Invar tube diameter	1 mm

Table 2. The parameters used in simulation

263 The statistical fluctuation in the electronic signal generated in a PMT for a certain number
 264 of incident photon is taken into account. The R8520 PMTs have 20% probability for double
 265 photoelectron emission for 178 nm photons, which is included in the simulation. Each detected
 266 photon on a PMT is assigned a uniform position on the PMT surface. The direction of this point
 267 with respect to the center of the LXe sphere is defined as the incident direction of the photon. The
 268 direction information is then used to calculate the angles between all possible pairs of photon for
 269 any event and calculate the correlation between all angle pairs.

270 In order to quantify the anisotropy of the emission, the angle correlation distribution of an
 271 anisotropic hit pattern is compared to that of the isotropic pattern. A χ^2 test statistic is used where
 272 the reduced χ^2 is defined as

$$\chi_{\nu}^2 = \frac{1}{\nu} \sum_{i=1}^{\nu} \frac{(O_i - E_i)^2}{E_i}, \quad (4.2)$$

273 where E_i is the expected number of entries for an isotropic emission obtained from a sample of
 274 10^5 simulated events. O_i is the observed number of entries, and ν is the total number of angle
 275 correlation bins which is also the number of dof . Sixty bins of identical width are used.

276 To asses the needed exposure to claim discovery assuming one of the patterns mentioned above,
 277 10^4 data sets are generated and tested against the null hypothesis. This is repeated for increasing
 278 number of events between 1 – 4000 assuming different values of the anisotropy fraction (r_{aniso}).
 279 The $\langle \chi_{\nu}^2 \rangle$ and its 2σ band for pattern 1, assuming $r_{aniso} = 0.1$ overlaid with the corresponding
 280 values for an isotropic emission are shown in Fig. 10. The values of N' , required to claim 5σ

discovery, for different values of r_{aniso} are calculated for each pattern as illustrated in Fig. 11. The number of events N' for $r_{aniso} = 0.1$ are summarized in Table 1 for all emission patterns.

A simulation with two typical sources that emit isotropically, a $10 \mu\text{Ci}$ ^{137}Cs (662 keV gamma), and a $2.7 \mu\text{Ci}$ AmBe (5 MeV neutron), shows that for an average yield of produced 50 photons/event, the rate of events in the detector is: 1.25×10^4 events/day for NR and 625 events/day for ER. Therefore a system that can operate stably for few weeks is expected to do reasonable measurements for ER and NR events.

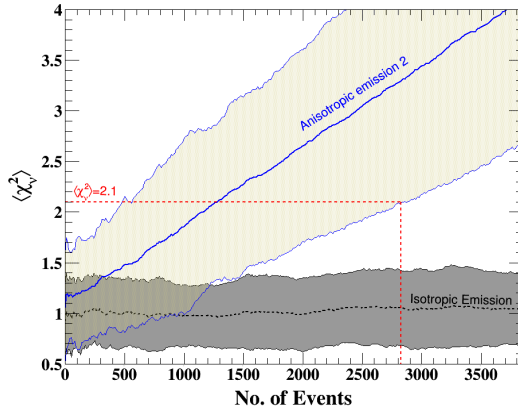


Figure 10. $\langle \chi^2_\nu \rangle$ and its 2σ band for isotropic emission (black) and for pattern 2 (blue). The $\langle \chi^2_\nu \rangle$ for isotropic emission fluctuate around 1 with $\sigma = 0.2$ which is consistent with the expected value of $\frac{1}{\sqrt{30}} \equiv 0.18$ for reduced χ^2 distribution with 60 degrees of freedom. ~ 3000 events are needed to claim 5σ discovery ($\chi^2_\nu = 2.1$) for this emission pattern

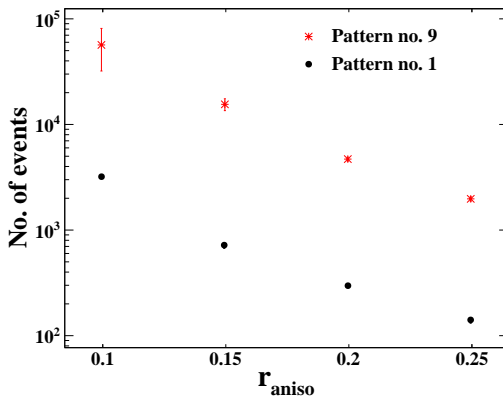


Figure 11. The number of events needed for an emission pattern to achieve 5σ presented only for pattern 1 and 9, for different values of r_{aniso} .

288 5 Commissioning runs

289 Maye change to the two features we want to measure is temporal and spatial; therefore, we
290 need stability (spatial) and fast response(temporal).

291 In order for this system to be able to measure *superradiance* effects there are two important
292 features the system needs to meet: stability and fast response. The estimated time for accumulating
293 data to achieve a 5σ effect assuming standard radioactive sources and some postulated emission
294 patterns(see Sec. 4)

295 **5.1 Stability Runs**

296 **5.2 Time resolution**

297 **6 Summary**

298 The setup of DIREXENO , an experiment to measure the spatial and temporal distribution of LXe
299 scintillation, has been presented. The system consists of 4 main building blocks (gas handling,
300 cryogenic, detector, and DAQ), each of which can be exchanged without altering others allowing
301 significant flexibility and modularity. Each of the building blocks has been described in detail, with
302 emphasis on the design and components.

303 The sensitivity of the setup to different postulated non isotropic emission patterns are studied
304 using MC simulations. For the patterns studied, a run-time of 2-3 weeks is required using typical
305 radioactive sources. Therefore the system is designed to maintain stability over a reasonable time
306 period.

307 Using DIREXENO , effects like superradiance or any other non-linear scintillation can be
308 measured. Measuring the correlation between the direction of the emission and the direction of the
309 radioactive source, may lead to directionality measurement which will allow enhanced statistical
310 modeling of background and improved sensitivity in DM experiments.

311 **References**

312 [1] Influx data. <https://www.influxdata.com>.

313 [2] Grafana labs. <http://grafana.com>.